Physica Medica 121 (2024) 103346

Contents lists available at ScienceDirect

Physica Medica

journal homepage: www.elsevier.com/locate/ejmp

Original paper

IOeRT conventional and FLASH treatment planning system implementation exploiting fast GPU Monte Carlo: The case of breast cancer

G. Franciosini [a,b], D. Carlotti [c], F. Cattani [d], A. De Gregorio [e,b], V. De Liso [f], F. De Rosa [a], M. Di Francesco [f], F. Di Martino [g,h,i,j], G. Felici [f], J. Harold Pensavalle [f,g,j], M.C. Leonardi [k], M. Marafini [l,b], A. Muscato [b,m], F. Paiar [g,i], V. Patera [a,b], P. Poortmans [n,o], A. Sciubba [a,p], A. Schiavi [a,b], M. Toppi [a,b], G. Traini [b], A. Trigilio [p,e], A. Sarti [a,b,*]

[a] Sapienza, University of Rome, Department of Scienze di Base e Applicate all'Ingegneria, Rome, Italy
[b] National Institute of Nuclear Physics, INFN, Section of Rome I, Rome, Italy
[c] Operative Research Unit of Radiation Oncology, Fondazione Policlinico Universitatio Campus-Bio Medico, Rome, Italy
[d] Unit of Medical Physics, European Institute of Oncology IRCCS, Milan, Italy
[e] Sapienza, University of Rome, Department of Physics, Rome, Italy
[f] S.I.T. Sordina IORT Technologies S.p.A, Aprilia, Italy
[g] Centro Pisano Multidisciplinare sulla Ricerca e Implementazione Clinica della Flash Radiotherapy (CPFR), Pisa, Italy
[h] University of Pisa, Department of Physics, Pisa, Italy
[i] Azienda Ospedaliero Universitaria Pisa (AOUP), Fisica Sanitaria, Pisa, Italy
[j] National Institute of Nuclear Physics, INFN, Section of Pisa, Pisa, Italy
[k] Division of Radiation Oncology, European Institute of Oncology IRCCS, Milan, Italy
[l] Museo Storico della Fisica e Centro Studi e Ricerche "E. Fermi", Rome, Italy
[m] Specialty School of Medical Physics, La Sapienza University of Rome, Rome, Italy
[n] Department of Radiation Oncology, Iridium Netwerk, Antwerp, Belgium
[o] University of Antwerp, Faculty of Medicine and Health Sciences, Antwerp, Belgium
[p] National Institute of Nuclear Physics, INFN, Frascati National Laboratories (LNF), Rome, Italy

ARTICLE INFO

Keywords:
IOeRT
TPS
GPU
Monte Carlo
FLASH
Breast cancer
IORT
Partial breast irradiation

ABSTRACT

Partial breast irradiation for the treatment of early-stage breast cancer patients can be performed by means of Intra Operative electron Radiation Therapy (IOeRT). One of the main limitations of this technique is the absence of a treatment planning system (TPS) that could greatly help in ensuring a proper coverage of the target volume during irradiation. An IOeRT TPS has been developed using a fast Monte Carlo (MC) and an ultrasound imaging system to provide the best irradiation strategy (electron beam energy, applicator position and bevel angle) and to facilitate the optimisation of dose prescription and delivery to the target volume while maximising the organs at risk sparing. The study has been performed in silico, exploiting MC simulations of a breast cancer treatment. Ultrasound-based input has been used to compute the absorbed dose maps in different irradiation strategies and a quantitative comparison between the different options was carried out using Dose Volume Histograms.

The system was capable of exploring different beam energies and applicator positions in few minutes, identifying the best strategy with an overall computation time that was found to be completely compatible with clinical implementation. The systematic uncertainty related to tissue deformation during treatment delivery with respect to imaging acquisition was taken into account.

The potential and feasibility of a GPU based full MC TPS implementation of IOeRT breast cancer treatments has been demonstrated in-silico. This long awaited tool will greatly improve the treatment safety and efficacy, overcoming the limits identified within the clinical trials carried out so far.

* Corresponding author at: Sapienza, University of Rome, Department of Scienze di Base e Applicate all'Ingegneria, Rome, Italy.
E-mail address: alessio.sarti@uniroma1.it (A. Sarti).

https://doi.org/10.1016/j.ejmp.2024.103346
Received 5 February 2024; Received in revised form 13 March 2024; Accepted 1 April 2024

1. Introduction

Among the different cancer treatment modalities available today, Intra Operative Radiation Therapy, delivered with electrons (IOeRT), can be used to effectively deliver the prescribed dose to the target volume maximising the local treatment efficacy decreasing the risk of local cancer recurrence [1–7]. Beside the use of electrons, recently, also the use of low energy X-rays is gaining attention in the context of local treatment of resected brain metastases [8].

In IOeRT the treatment is delivered directly to the primary tumour bed and the clinical workflow is detailed as an example for the most frequent treatment: partial breast irradiation (PBI) [9–15].

The possibility to implement dedicated shielding, exploiting the surgical breach, can increase furthermore the sparing of Organs At Risk (OARs): protective disks, whenever possible and needed, can be inserted by the surgeon to additionally shield OARs that are close to the target volume. For the PBI case, such organs are mainly the ribs, lungs and heart that might be adjacent to the target volume [16–20]. Whenever the tissues that have to be treated are ready, their thickness is measured with a graduated needle and the energy of the electrons is assessed accordingly. The patient is then treated with a single irradiation of mono-energetic electrons delivered within less than 2 min (Averaged Dose Rate is >10 Gy/min), being the typical prescription 21 Gy at 90% isodose [21], by means of a compact linear accelerator and an applicator that allows to achieve the desired dose flatness and conformity to the target. Once treated, the protective disk is removed, the breach is closed and the surgery ends.

The treatment planning, up to now, was not foreseen in the clinical workflow for two main fundamental reasons: the lack of 'intra-operative' imaging, needed to allow for the dose calculation, and the time needed to produce dose maps that could be used for an optimisation process. The absorbed dose in these cases was simply assessed by means of an analytical calculation. An IORT-dedicated imaging and Treatment Planning System (TPS) has been sought with great efforts, but despite the significant research activity [22–30] no solutions adaptable to a routinely use in the clinical practice, capable of including an intra-operative imaging input for the planning, have been developed so far. Instead a solution, the Radiance planning tool, that is based on pre-surgery imaging information has been developed and made available to the interested therapy centres [31]. In this case a hybrid Monte Carlo algorithm is used to simulate the dose in homogeneous and heterogeneous media and Cone Beam CT images acquired after surgery, whenever available, can be used to perform the tissue heterogeneity correction [28].

The outcome of the treatments carried out as previously detailed has been evaluated in the context of different clinical trials. The risk analysis performed to evaluate the possibility of local recurrences and documented in the ELIOT [21,32] clinical trial, demonstrated that outcomes after IOeRT-based PBI were not optimal, what has been linked to underdosage or geographical miss of the Clinical Target Volume (CTV) due to absence of proper imaging, treatment planning and applicator docking or position checking. Such findings have been documented in a manuscript with specific recommendations for breast cancer IOeRT treatments [10].

The findings of ELIOT trial can be explained in view of two specific aspects of the workflow: the absence of a treatment planning tool for the assessment of target coverage with a given applicator configuration and the need to keep the surgical breach to insert the protective disk to a minimum dimension as surgeons are not willing to practice wide cuts for the removal of small tumours as this appeared to be unnecessary and it impacts on patient cosmesis. As an example we discuss the case of a 1.5 diameter tumour (CTV). Assuming that a margin of 2 cm is applied when defining the Planning Treatment Volume (PTV) to ensure the proper treatment of the tissue that is not removed, and that a circular applicator (external ⌀ = 7 cm, to account for additional uncertainties related, e.g. to the positioning) is needed to treat the volume, an incision of 10.5 cm will be needed. Surgeons usually prefer not to practice such large incisions, the applicator diameter is reduced accordingly resulting in an under-dosage of the PTV. In addition, the positioning of the applicator that is used to deliver the beam to the primary tumour bed is done by the radiotherapist once the breach is closed without any machine guided help increasing significantly the risk of geographical misses.

These limitations could be overcome using a TPS provided with an image guided docking technology capable of reducing the positioning uncertainties and the risk of geographical misses [31,33]. The feasibility of introducing a dedicated fast Monte Carlo (MC) simulation in the clinical workflow was already explored in [34], proving that a Central Processing Unit (CPU) based solution was capable of providing reliable results in a time scale of few minutes. However, the exploration of different configurations and the task of plan optimisation remained difficult in the short time available after the tumour resection. In the following we discuss the possibility of using an ultrasound (US) scanner to acquire, after-surgery, the image of the tissues to be treated, define the CTV, PTV and OARs to compute, using a GPU-based Monte Carlo (MC) software the absorbed dose maps needed for the optimisation process and perform a full treatment plan optimisation.

Such planning tool becomes additionally interesting in view of the recent experimental evidence of OARs sparing is presence of treatments delivered at ultra high dose rates (>40 Gy/s, FLASH effect [35–43]). The use of monoenergetic high-intensity pulses of electrons (needed to deliver as fast as possible the whole dose of several Gy) makes IOeRT the current best candidate for the first clinical implementation of the FLASH effect.

Exploiting the FLASH effect could help the surgeons to avoid invasive surgery procedures, i.e. large surgical breaches, which can increase postoperative complications and pain and produces visible scars while maintaining the treatment efficacy [44,45].

The solutions that have been foreseen, implemented and tested by means of an in-silico study are detailed in Section 2. Section 3 presents the results obtained in a PBI case delivered both in conventional (~0.05–0.5 Gy/s) and FLASH dose rate regimes. The impact on the future of IOeRT breast cancer treatments is finally discussed in Section 4.

2. Materials and methods

The IOeRT planning that we have implemented, starts from the anatomical and geographical information on the tissues that have to be treated that has to be acquired by means of an imaging technique. Then MC simulation is used to compute the absorbed dose inside the tissues and different irradiation configurations are explored to ensure the target volume coverage and maximise the OARs sparing. The latter evaluation is performed by means of Dose Volume Histograms (DVHs).

The current IOeRT clinical workflow does not foresee any post-resection imaging. One possibility, in the future, could be to have a technology capable of performing a fast CT scan during surgery in the actual conditions used to deliver the beam. As this technology is currently not foreseen or available during standard IOeRT treatments, we have explored a customised solution utilising ultrasound imaging. This system enables the acquisition of a 3D image by performing a vectorial sum of 2D US images obtained through a US probe, which is spatially monitored in real-time using an optical tracker. This solution allows to acquire the position of the tissues after the tumour resection and the eventual implantation of a protective disk.

In this case, as shown in Fig. 1, the IOeRT clinical workflow becomes as follows: (i) the patient undergoes the resection; (ii) the surgeon and the radiation oncologist define and prepare the volume to be treated and inserts the protection disk whenever needed; (iii) the US probe is used to acquire an image of the tissues and the positioning of the protection disk with respect to a general reference point known to the accelerator positioning device; (iv) the surgeon and the radiation

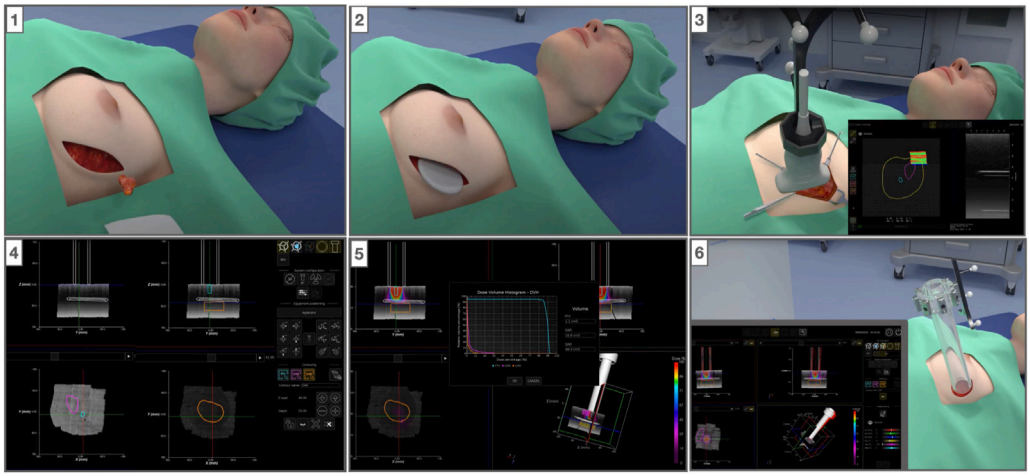

Fig. 1. IOeRT procedure: (1) the patient is surgically treated and the tumour mass is removed; (2) whenever needed a radio-protection disk is inserted under the area that will be irradiated; (3) by using a US probe, which is referenced in the space by means of an optical tracker, the surgeon acquires US images; (4) the surgeon identifies the surface to be scanned and regions of interest (PTV and OARs); (5) different treatment configuration are explored looking for the optimal one. The whole process takes less than 2 min. At the end image guided docking is correctly performed and the dose is recalculated (6).

oncologist define the target volume (PTV) and OARs positions using the software interface that displays the ultrasound output; (v) the treatment planning is performed exploring different beam applicator positions, angles and energies; (vi) the accelerator and the applicator are placed by the radiation oncologist in the optimised position and the plan is delivered. Image guidance helps docking process and the dose distribution and DVH are calculated again when docking is over to minimise the risk of geographical miss.

To test the workflow and assess the feasibility of a fast optimisation of the treatment plan during surgery, a MC study has been performed. FRED, the GPU-accelerated [46–48] dose engine used to compute the dose maps, implements all the necessary electromagnetic processes needed to reach the accuracy required for the planning and allows to compute the maps within seconds. By using a full MC implementation we were able to test the feasibility of a plan optimisation whenever a CT of the patient would become available and the use of actual tissue densities would have a larger impact on the final plan and dosimetric report precision. However, to test the workflow in the worst case scenario, we used for our simulations a modified phantom in which the US information was used to mimic the real conditions of a clinical IOeRT treatment workflow, implying that only water, air and the Radio-Protection disc (RPD) materials were allowed and the US input was used to define the simulation geometry. To perform all the simulations presented in our manuscript we used an NVIDIA GeForce RTX 3090 GPU. As patient related US imaging data are not yet available, in our study we used a CT image of an anthropomorphic RANDO® male phantom with a silicone breast prosthetic application, modified to account for the expected US position resolution. All the voxels belonging to the patient were assigned to the water Hounsfield unit (HU) while outside the patient the air HU was used. According to the US expected imaging performance, we defined Regions Of Interest (ROIs) with a depth of no more than 7 cm (equal to the US optimal viewing).

The PTV was defined with an approximately spherical shape with a mean radius of 2.5 cm and its centre was placed at a depth of 3.8 cm from the phantom skin surface (Fig. 2 panel A, in red). This region has been defined accounting for the additional margin, with respect to the clinical target volume, usually defined by the surgeons in PBI treatments after the tumour resection. The studies presented here-after consider the presence of an RPD inserted just after the PTV, to protect the patient OARs (ribs, heart, lung). The disk is shown in panel A of Fig. 2, in white. We modified the HU value of the CT in order to define a cylindrical disk (radius of 3.9 cm) composed of a first layer, 3 mm thick, of Polytetrafluoroethylene (PTFE, HU = 950) and a second one, with the same thickness, of stainless steel (HU = 10 000) [17,49].

In addition to the PTV and RPD we defined additional OARs needed for the plan evaluation, all shown in panel A in Fig. 2. The phantom Skin region was defined starting from the edge between the materials identified, respectively, as water and air, with a thickness of 5 mm. The Pectoral Muscle region, was instead defined to evaluate the dose released after the RPD and designed as a cylindrical-shaped region with a thickness of 1.2 cm and a mean radius of 3.9 cm placed just after the RPD. Finally, the Breast region was defined as to include all the tissues between the phantom skin and the RP disk surrounding the PTV, with the latter being subtracted. To account for the surgical breaches and tissue deformation needed to insert the applicator, we directly replaced the water HUs with air up to a depth of 1.3 cm, according to the PTV and applicator dimension. In Fig. 2, panel A, the surgical breach is not shown.

Calculation and optimisation of the absorbed dose maps was performed assuming a dose prescription of 20 Gy covering the PTV along the beam direction and enclosing 90% of the PTV along the radial directions.

For the treatment optimisation different configurations were explored: beam energies, applicator sizes and positions were simulated assuming FLASH or conventional delivery conditions.

The best plan was selected by calculating the Dose Volume Histograms (DVH) after each simulation. Once all the simulations are completed, the TPS is able to determine the best configuration minimising the absorbed dose to the OARs while ensuring the proper PTV coverage.

2.1. Selecting the best plans

While a full MC simulation of a plan optimised to deliver 20 Gy to the PTV would imply the study of $\sim 10^{12}$ electron interactions, the simulations were performed using only 510^5 primary electrons. To define the optimal statistics needed to ensure robust results against statistical fluctuation, the DVH for a given plan have been re-obtained for different number of electrons in the range between 10^4 and 10^6. The absorbed dose distribution in each voxel was averaged with the values of its adjacent neighbours to minimise the impact of single voxel fluctuations. The total number of 510^5 represented a good compromise between the overall simulation time, which has to be compatible with the whole time available during the surgery (few minutes) for the full plan calculation and optimisation, and the overall DVHs robustness. As

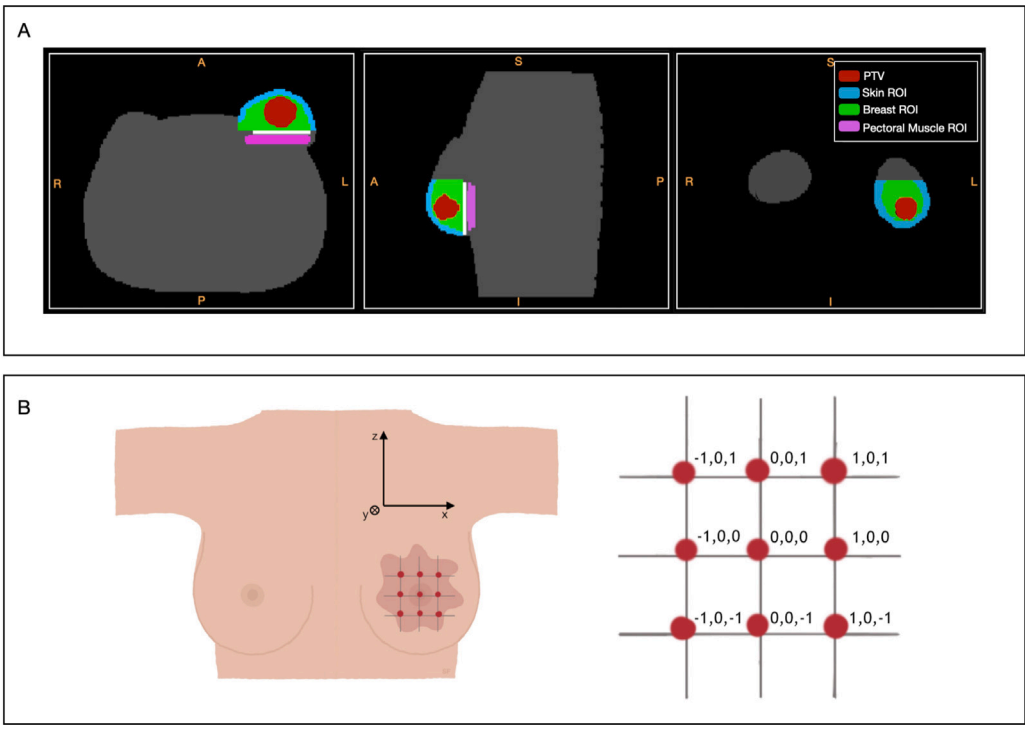

Fig. 2. Panel A: Visualisation of the three anatomical planes, transverse, sagittal and frontal respectively, of the anthropomorphic phantom. The CT has a voxels dimension of 0.2 cm in all the directions. The ROIs are also highlighted: the PTV in red, the skin ROI in blue and the Breast and Pectoral Muscle ROI in green and purple, respectively. In white the RP disk with diameter equal to 40 mm, is also shown. Panel B: Schematic view of the position scan. The centre of the beam, impinging on the phantom along the *y* direction, was moved in a [x,z] grid with 10 mm steps. Starting from the centred position ([0,0]), nine different simulations were performed with the beam centre located on the red dots. (For interpretation of the references to colour in this figure legend, the reader is referred to the web version of this article.)

the GPU hardware is already exploited to its highest power, increasing the statics without adding additional hardware resources, would result in an increased processing time, with an almost linear dependence of the total simulation time with respect to the number of primaries generated. We defined the final value as the smallest one from which the statistical fluctuations among the DVHs performed with different random seeds became negligible. In these conditions, the dose in each voxel fluctuates with an average relative uncertainty of 1%.

The overall procedure of computing the absorbed dose map needs to proceed quickly enough to allow for a plan optimisation within the limited amount of time available after the surgery. Using FRED we were able to perform the full simulation of the interactions of 510^5 electrons from an 8 MeV beam (80 mm applicator diameter) impinging on the modified CT in only eight seconds (including the DVHs calculation time).

The choice made on the ranges of energies, positions and applicator diameters to be explored is based on the clinical experience of PBI treatments. Based on the dimension, position and thickness of the PTV considered in our simulations, we defined 8, 10 and 12 MeV as options to be investigated for the beam energy.

Concerning the applicator size, we proceeded as in the clinical practice, exploring the range of dimensions that guarantees the best compromise between the PTV coverage and the surrounding healthy tissues sparing. The minimum size of the applicator diameter was set relative to the size of the PTV dimension in the transverse plane with respect to the beam direction (40 mm ⌀), to ensure the minimum coverage of the target volume, neglecting the additional safety margins that are important to reduce the risk of local recurrences. The upper limit, instead, was defined as to properly account for the additional margins around the PTV. Margins of 0.5, 1 and 1.5 cm were considered, resulting in the study of applicators with diameters of 50, 60 and 70 mm, respectively. The study of maximum applicator size plays a crucial role when trying to maximise the treatment efficacy.

Finally, the optimisation of the applicator position was performed by means of a scan around the surgical breach. The beam centre, impinging on the phantom along the *y* direction, was moved from the centred position [0,0] in a (x,z) grid with 10 mm steps, as shown in panel B of Fig. 2. As for the other studies, the DVHs have been computed to find the optimal configuration.

3. Results

The isodose maps obtained for electron beam energies of 8, 10 and 12 MeV and using a 50 mm internal diameter applicator are shown in Fig. 3 (panel A) while in Fig. 4 (Left) the corresponding DVHs are reported. To match the dose prescription, the dose maps produced by FRED in Gy/primary units, were multiplied by the number of electrons required to ensure the dose prescription at the PTV (20 Gy at 90% of the PTV volume). From the DVH, it is possible to see that the 8 MeV beam does not provide an adequate PTV coverage defined as, here and in the following, the fraction of the PTV volume that receives 95% of the prescribed dose (V95). In this case, the values of V95 for the three energies are, respectively, 92%, 96% and 97% for 8, 10 and 12 MeV energies.

The results obtained for 12 MeV clearly show that at such energy the dose absorbed by the pectoral muscle region grows significantly. The results for 10 MeV show that a proper PTV coverage at the cost of a small dose to the pectoral muscle ROI and for that reason the 10 MeV energy has been chosen as reference for the other studies.

The results of the applicator diameter optimisation study are shown in Fig. 3 (panel B) and Fig. 4 (Right). The results have been obtained using a fixed beam energy of 10 MeV. The DVHs are clearly showing that when using a 40 mm internal diameter, it is not possible to achieve the required PTV coverage with V95 values for the different applicator dimensions that are, respectively, 93%, 96%, 96% and 97%.

The dose to breast and skin increases as expected when using larger applicators, accordingly with the geometry and positioning of the ROIs.

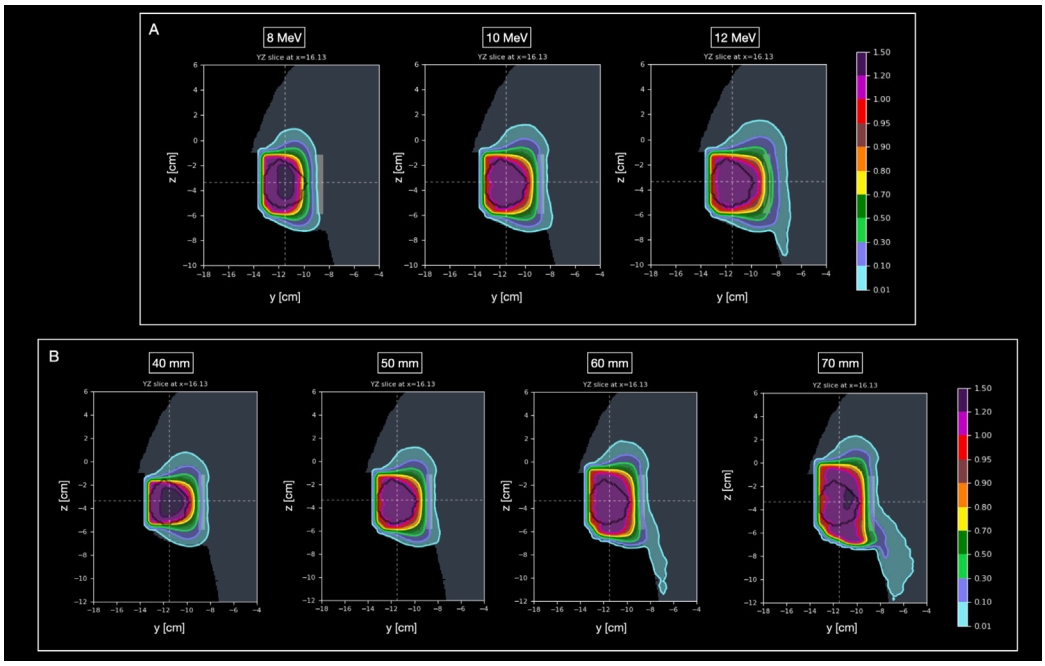

Fig. 3. Isodose maps comparison using different beam energies (panel A) and applicator dimensions (panel B) for the simulation. The first scan was obtained from the IOeRT plan, respectively, with 8, 10 and 12 MeV electron beams collimated by a 50 mm diameter applicator, whereas the second one was obtained by changing only the applicator dimension (ranging from 40 to 70 mm) with a fixed beam energy equal to 10 MeV. The dose levels below 1% of the prescribed dose, i.e. 20 Gy, were masked for enhancing clarity in visualisation. The absorbed dose in Gy/primary units were normalised to match the dose prescription. The PTV is also highlighted with a dotted black curve.

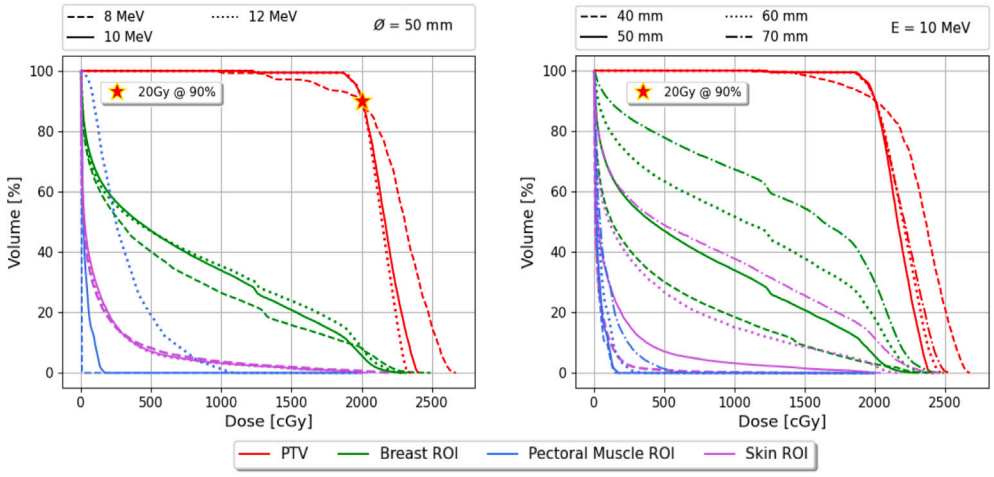

Fig. 4. Plan comparison with different beam energies and applicator dimensions. DVHs for the PTV and OARs obtained from the IOeRT plan with an 8, 10 and 12 MeV electron beam collimated by a 50 mm diameter applicator are reported on the left, whereas the ones obtained by changing only the applicator dimension (ranging from 40 to 70 mm) with a fixed beam energy equal to 10 MeV are shown on the right. The absorbed dose in Gy/primary units were normalised to match the dose prescription.

The position scan study was performed using electrons with 8 MeV energy and an applicator of 50 mm internal diameter. The simulation was performed for the nine different beam positions shown by the red dots in Fig. 2, panel B. The DVHs obtained for each position are shown in panel A of Fig. 5 left and right, respectively, for the PTV and Breast region. Panel B of the same figure, shows the dose maps in Gy units for the centred and worst-case plans, corresponding to the [0,0] and [1,1] positions, respectively, as illustrated in panel B of Fig. 2.

The best plan selection algorithm implements the calculation of mean and maximum doses in the OARs and returns, in each scan, the optimal configuration ensuring the proper PTV coverage while lowering the dose to the OARs as much as possible.

3.1. TPS timing performance

The plan calculation and optimisation time for the study of the beam energy lasted 13 s, the diameter optimisation study took 16 s and finally the scan of 9 positions in the transverse plane with respect to the beam direction required 35 s.

Assuming that different geometrical configurations could be explored by the radiation oncologists, at different energies, the timing performance shown before are demonstrating that up to 50 different simulations could be doable on a single GPU cards within the allowed time (few minutes). As an example, the simulation time needed to explore three different beam energies and, for each energy, three different

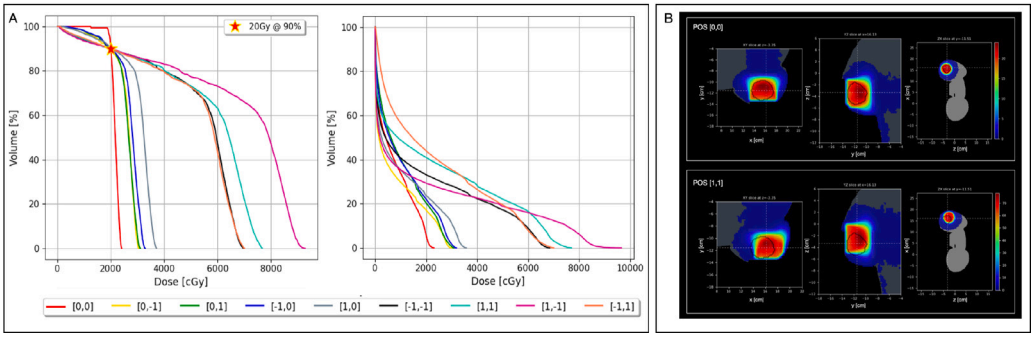

Fig. 5. Panel A: DVHs for the PTV (left) and Breast ROI (right) for the nine simulations. The centred position corresponds to the [0,0] simulation while the others are identified by the coordinates shown in Fig. 2, panel B. All dose maps were multiplied by the number of electrons needed to match the dose prescription, $\sim 10^{12}$. Panel B: Dose maps comparison between the centred (upper) and worst-case (bottom) plans, corresponding to the [0,0] and [1,1] positions, respectively, as defined in panel B of Fig. 2. The PTV is highlighted with a dotted black curve. The dose maps in Gy/primary units were multiplied by the number of electrons needed to match the dose prescription.

applicator positions, is ~1 min. Such time can be further reduced by increasing the number of GPUs.

3.2. The FLASH effect potential

The PBI treatment is undeniably one of the most suited for meeting the requirements needed to trigger the FLASH effect: very high dose rates can be easily achieved, and the monoenergetic, high dose irradiation is performed to deliver 20 Gy in a single fraction. We thus expect a significant contribution from the FLASH effect. However, the main difficulty is related to the evaluation of the FLASH effect potential when trying to account for the large experimental uncertainties that are yet affecting the evaluation of the OARs sparing in UHDR regimes. In our study we have implemented the FLASH-modifying factor (FMF) model that was introduced by Bohlen et al. in [50]. According to the dose absorbed by each voxel in the full treatment, an FMF re-weighed dose (DFMF) has been calculated and the DFMF Volume Histograms have been computed and compared with the ones obtained in conventional irradiation.

The values of FMF^{min} and D_{Th}, that refer in the model as the maximum sparing achievable at very high doses and the minimum threshold that has to be crossed in order to trigger the effect, have been taken as from the ones measured in *in vivo* experiments reported in detail in [50]. Considering the results from pooled mammalian skin treatments [51] we were able to define $D_{Th} = 16.6$ Gy and $FMF^{min} = 0.5$ (see table 2 in [50]) and used these values in the following to assess the FLASH effect potential. While these values can represent a reasonable assumption to evaluate, as of today, the potential of FLASH irradiation, an additional effort would be needed in the future to decrease the large uncertainties affecting the data sample used for the modelling to provide results that are more robust.

The results obtained with a protection disk and an applicator with the internal diameter, respectively, of 40 and 50 mm are shown in dashed and dotted lines in Fig. 6 for a conventional irradiation. In these cases, the applicator and RPD dimensions were properly matched, as the OARs have to be directly spared using the RPD. Solid lines are showing the results obtained delivering the plan at UHDR and implementing the FLASH effect sparing.

The configuration explored still implements a RPD and a surgical breach with a diameter of 40 mm but instead an applicator of 50 mm diameter partially superimposed to the skin is used. This study was performed to show the potential of the FLASH effect to produce results that are comparable, or even better, than the ones achieved with a larger RPD but with a smaller surgical breach with respect to the conventional irradiation. Fig. 6 shows that the OARs that absorb a dose above the selected threshold, in FLASH configuration, have reduced effective doses, when compared to the CONV 50/50 configuration, defined as the one in which the applicator diameter is 50 mm large, exactly matching the surgical breach.

The DFMF Volume Histograms obtained could hence be a valuable tool in the hands of the radiation oncologists to assess the real need of a RPD and its dimensions, helping to ensure that a proper PTV coverage is reached while keeping the effective dose below the identified limits.

4. Discussion

The results obtained when performing a plan optimisation of a PBI treatment prove the feasibility of a DVH based approach to the identification and selection of the most optimal IOeRT set-up. The absorbed dose maps can be obtained quickly enough and the study of the dose tails as shown in Figs. 5, 4 and 6 can be used to identify the plan that ensures the required PTV coverage while minimising the dose to the OARs.

The obtained results are underlining the importance of an automated procedure that can identify the best treatment position and ensure, via the image guided docking of the applicator, that the treatment corresponds to what has been planned. This is especially true in the context of IOeRT treatments in which the geographical misses have been reported as the main cause of treatment limited efficacy. Fig. 5 clearly shows the crucial role played by the applicator positioning and its impact in ensuring the proper, full, PTV coverage.

The statistics used to obtain the dose maps allowed to minimise the impact of statistical fluctuations while keeping the calculation time on one single GPU below 10 s. Depending on the time available after the US imaging is acquired, different energies beam positions and applicator size can be investigated helping the radiation oncologists finding the best treatment strategy.

The described clinical workflow becomes particularly interesting in the context of recent studies that demonstrated the efficiency of IOeRT treatment during laparoscopic, thoracoscopic, and robotic-assisted surgical procedures [37]. Such minimally invasive surgery could significantly improve the tolerance for surgical procedures in cancer patients, while maintaining established quality standards in cancer surgery.

The feasibility of such treatments, in which the applicator needs to be placed directly on the skin and the RPD is missing can be evaluated by means of a dedicated TPS optimisation study as described above taking into account the advantage from the possibility of delivering the beam at ultrahigh dose rates exploiting the FLASH effect.

The availability of a full MC tool capable of evaluating the biological dose will allow to explore the possibility to avoid the insertion of protective disks, or placement of the applicator inside the surgical breach, to account for the reduced damage to organs and skin achievable at FLASH rates. The surgeons and the radiation oncologists will be able to explore different treatment strategies, ensuring a proper target coverage while minimising the damage to the healthy tissues, fully exploiting the potential of IOeRT irradiations.

The results and technique presented so far assumed an US-based imaging input. As the software can use a CT image as input, the impact

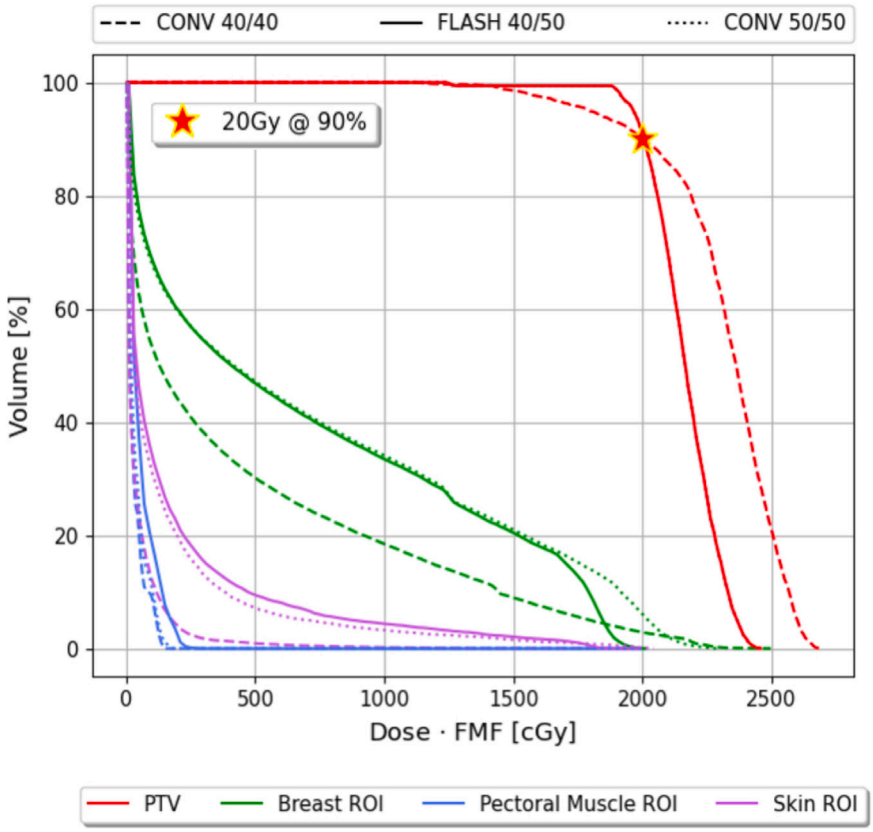

Fig. 6. Biological effective dose volume histograms for the PTV (red), Breast ROI (green), Pectoral Muscle ROI (blue) and Skin (purple) for the simulations performed in conventional regime (CONV) with a 40 mm (dashed line, 40/40) and 50 mm (dotted line, 50/50) surgical breach and applicator dimension, and in FLASH regime with a small surgical breach 40 mm, and a larger applicator diameter 50 mm (solid line, 40/50). The DFMF was obtained by multiplying the physical dose for the dimensionless FMF factor (see [50]), which for conventional treatment was set to 1. (For interpretation of the references to colour in this figure legend, the reader is referred to the web version of this article.)

of an improved imaging has been tested and was found to have a negligible impact on the selection of best plan for PBI treatments. The actual densities measured during the phantom CT were used in the dose calculation, while the ROI definition remained the same. This study, hence, does not take into account the impact of an improved image quality in defining the PTV and OARs regions.

As a systematic cross-check of the results, different geometries have been implemented to test the effect of a possible tissue deformation whenever the applicator is placed in the treatment position, with respect to what has been acquired with the US system without any applicator. The tissue shape has been modified, removing part of the tissue placed on the applicator edge (few mm) and changing the width of the tissue traversed before the PTV (few mm). All the obtained results are consistent with the identification of the best plan presented in Section 3, demonstrating the robustness of the procedure against small deformation of the tissue following the placement of the applicator.

Finally, it is important to stress that once the hardware will be fully available (implementing both the image guided positioning of the applicator and the integration with the ultrasound probe) the whole process validation using a dedicated phantom will be the subject of a dedicated paper.

5. Conclusions

The possibility to compute and optimise an IOeRT plan within a few minutes using a single GPU card has been demonstrated. The average dose values and the DVHs for each ROI can be made available to the radiation oncologists and breast surgeon for checking the different options and a final, fast, absorbed dose calculation can be performed as soon as the final positioning, energy and beam configurations will be defined by the operator and validated by the image guided docking system. Hereby, the level of treatment preparation, recording and verification for IOeRT procedures approaches the level as in use for external beam RT.

The proposed clinical workflow will allow the radiation oncologist and breast surgeon to evaluate the real need of an RPD insertion and to evaluate the dose distribution and PTV coverage when changing the applicator diameter, providing all necessary information needed to define the irradiation geometry and avoid PTV under-dosage. In addition, it will also be possible to provide the necessary certification for the dose absorbed by the patient, as needed for each radiation treatment by many countries.

Finally, the software tools can help exploring the potential of UHDR irradiations. For PBI the FLASH effect represent an excellent opportunity, having the potential to re-define the workflow for IOeRT treatments allowing to place the applicator directly on part of the patient skin and/or avoiding the use of RPD. This would imply a surgical procedure that is far less invasive and offers a better quality of life for the patient. The implementation of the TPS that we have proposed, that is capable of properly accounting for the FMF correction, is the key that will enable such advancement in the clinical workflow.

Declaration of competing interest

The authors declare the following financial interests/personal relationships which may be considered as potential competing interests: Alessio Sarti reports financial support was provided by S.I.T. Sordina IORT Technologies S.p.A. Vincenzo Patera reports financial support was provided by S.I.T. Sordina IORT Technologies S.p.A. If there are other authors, they declare that they have no known competing financial interests or personal relationships that could have appeared to influence the work reported in this paper.

Acknowledgements

This work has been partially funded by CSN5 of INFN in the context of the FRIDA project.

References

[1] Calvo F. Intraoperative irradiation: Precision medicine for quality cancer control promotion. Radiat Oncol 2017;12(1). http://dx.doi.org/10.1186/s13014-017-0764-5, cited By 16.

[2] Valentini V, Calvo F, Reni M, Krempien R, Sedlmayer F, Buchler MW, Di Carlo V, Doglietto GB, Fastner G, Garcia-Sabrido JL, Mattiucci G, Morganti AG, Passoni P, Roeder F, D'Agostino GR. Intra-operative radiotherapy (IORT) in pancreatic cancer: Joint analysis of the ISIORT-europe experience. Radiother Oncol 2009;91(1):54–9. http://dx.doi.org/10.1016/j.radonc.2008.07.020.

[3] Calvo FA, Sole CV, Rutten HJ, Dries WJ, Lozano MA, Cambeiro M, Poortmans P, González-Bayón L. ESTRO/ACROP IORT recommendations for intraoperative radiation therapy in locally recurrent rectal cancer. Clin Transl Radiat Oncol 2020;24:41–8. http://dx.doi.org/10.1016/j.ctro.2020.06.007.

[4] Roeder F, Morillo V, Saleh-Ebrahimi L, Calvo FA, Poortmans P, Ferrer Albiach C. Intraoperative radiation therapy (IORT) for soft tissue sarcoma – ESTRO IORT Task Force/ACROP recommendations. Radiother Oncol 2020;150:293–302. http://dx.doi.org/10.1016/j.radonc.2020.07.019.

[5] Calvo FA, Asencio JM, Roeder F, Krempien R, Poortmans P, Hensley FW, Krengli M. ESTRO IORT Task Force/ACROP recommendations for intraoperative radiation therapy in borderline-resected pancreatic cancer. Clin Transl Radiat Oncol 2020;23:91–9. http://dx.doi.org/10.1016/j.ctro.2020.05.005.

[6] Calvo FA, Krengli M, Asencio JM, Serrano J, Poortmans P, Roeder F, Krempien R, Hensley FW. ESTRO IORT Task Force/ACROP recommendations for intraoperative radiation therapy in unresected pancreatic cancer. Radiother Oncol 2020;148:57–64. http://dx.doi.org/10.1016/j.radonc.2020.03.040.

[7] Haddock M. Intraoperative radiation therapy for colon and rectal cancers: A clinical review. Radiat Oncol 2017;12(1). http://dx.doi.org/10.1186/s13014-016-0752-1, Publisher Copyright: © 2017 The Author(s).

[8] Diehl CD, Pigorsch SU, Gempt J, Krieg SM, Reitz S, Waltenberger M, Barz M, Meyer HS, Wagner A, Wilkens J, Wiestler B, Zimmer C, Meyer B, Combs SE. Low-energy X-Ray intraoperative radiation therapy (Lex-IORT) for resected brain metastases: A single-institution experience. Cancers 2023;15(1). http://dx.doi.org/10.3390/cancers15010014, URL https://www.mdpi.com/2072-6694/15/1/14.

[9] Stefanelli A, Farina E, Mastella E, Fabbri S, Turra A, Bonazza S, De Troia A, Radica MK, Carcoforo P. Full-dose intraoperative electron radiotherapy for early breast cancer: Evidence from a single center's experience. Cancers 2023;15(12). http://dx.doi.org/10.3390/cancers15123239.

[10] Fastner G, Gaisberger C, Kaiser J, Scherer P, Ciabattoni A, Petoukhova A, Sperk E, Poortmans P, Calvo FA, Sedlmayer F, Leonardi MC. ESTRO IORT Task Force/ACROP recommendations for intraoperative radiation therapy with electrons (IOERT) in breast cancer. Radiother Oncol 2020;149:150–7. http://dx.doi.org/10.1016/j.radonc.2020.04.059.

[11] Correa C, Harris EE, Leonardi MC, Smith BD, Taghian AG, Thompson AM, White J, Harris JR. Accelerated partial breast irradiation: Executive summary for the update of an ASTRO evidence-based consensus statement. Pract Radiat Oncol 2017;7(2):73–9. http://dx.doi.org/10.1016/j.prro.2016.09.007.

[12] Fastner G, Reitsamer R, Gaisberger C, Hitzl W, Urbański B, Murawa D, Matuschek C, Budach W, Ciabattoni A, Reiland J, Molnar M, Vidali C, Schumacher C, Sedlmayer F, on behalf of the HIOB Trialist Group. Hypofractionated whole breast irradiation and boost-IOERT in early stage breast cancer (HIOB): First clinical results of a prospective multicenter trial (NCT01343459). Cancers 2022;14(6). http://dx.doi.org/10.3390/cancers14061396.

[13] Kaidar-Person O, Meattini I, Zippel D, Poortmans P. Apples and oranges: comparing partial breast irradiation techniques. Rep Pract Oncol Radiother 2020;25(5):780–2. http://dx.doi.org/10.1016/j.rpor.2020.07.008.

[14] Bentzen SM, Haviland JS, Yarnold JR. Targeted intraoperative radiotherapy for early breast cancer. JAMA Oncol 2020;6(10):1636. http://dx.doi.org/10.1001/jamaoncol.2020.2716.

[15] Piroth MD, Strnad V, Krug D, Fastner G, Baumann R, Combs SE, Duma MN, Dunst J, Feyer P, Fietkau R, Haase W, Harms W, Hehr T, Sedlmayer F, Souchon R, Budach W, Breast Cancer Expert Panel of the German Society of Radiation Oncology (DEGRO). Long-Term Results of the TARGIT-A Trial: More Questions than Answers. Breast Care 2021;17(1):81–4. http://dx.doi.org/10.1159/000515386.

[16] Severgnini M, de Denaro M, Bortul M, Vidali C, Beorchia A. In vivo dosimetry and shielding disk alignment verification by EBT3 GAFCHROMIC film in breast IOERT treatment. J Appl Clin Med Phys 2015;16(1):112–20. http://dx.doi.org/10.1120/jacmp.v16i1.5065.

[17] Robatjazi M, Baghani HR, Mahdavic SR, Felici G. Evaluation of dosimetric properties of shielding disk used in intraoperative electron radiotherapy: A Monte Carlo study. Appl Radiat Isot 2018;139:107–13. http://dx.doi.org/10.1016/j.apradiso.2018.04.037.

[18] Tarrats Rosell J, Cases C, Garcia-Causapié M, Trias G, Oses G, Herreros A, Molla M. PO-1774 design and in-silico evaluation of a breast IOERT aligner to prevent OAR irradiation. Radiother Oncol 2023;182:S1494–5. http://dx.doi.org/10.1016/S0167-8140(23)66689-7, ESTRO 2023, 13 - 16 May 2023, Vienna, Austria.

[19] Righi S, Karaj E, Felici G, Di Martino F. Dosimetric characteristics of electron beams produced by two mobile accelerators, Novac7 and Liac, for intraoperative radiation therapy through Monte Carlo simulation. J Appl Clin Med Phys 2013;14(1):6–18. http://dx.doi.org/10.1120/jacmp.v14i1.3678.

[20] Leonardi MC, Maisonneuve P, Mastropasqua MG, Morra A, Lazzari R, Rotmensz N, Sangalli C, Luini A, Veronesi U, Orecchia R. How do the ASTRO consensus statement guidelines for the application of accelerated partial breast irradiation fit intraoperative radiotherapy? A retrospective analysis of patients treated at the European Institute of Oncology. Int J Radiat Oncol*Biol*Phys 2012;83(3):806–13. http://dx.doi.org/10.1016/j.ijrobp.2011.08.014.

[21] Orecchia R, Veronesi U, Maisonneuve P, Galimberti VE, Lazzari R, Veronesi P, Jereczek-Fossa BA, Cattani F, Sangalli C, Luini A, Caldarella P, Venturino M, Sances D, Zurrida S, Viale G, Leonardi MC, Intra M. Intraoperative irradiation for early breast cancer (ELIOT): long-term recurrence and survival outcomes from a single-centre, randomised, phase 3 equivalence trial. Lancet Oncol 2021;22(5):597–608. http://dx.doi.org/10.1016/S1470-2045(21)00080-2.

[22] Petoukhova A, Snijder R, Vissers T, Ceha H, Struikmans H. In vivodosimetry in cancer patients undergoing intraoperative radiation therapy. Phys Med Biol 2023;68,18. http://dx.doi.org/10.1088/1361-6560/acf2e4.

[23] García-Vázquez V, Sesé-Lucio B, Calvo FA, Vaquero JJ, Desco M, Pascau J. Surface scanning for 3D dose calculation in intraoperative electron radiation therapy. Radiat Oncol 2018;13:243. http://dx.doi.org/10.1186/s13014-018-1181-0.

[24] García-Vázquez V, Calvo FA, Ledesma-Carbayo MJ, Sole CV, Calvo-Haro J, Desco M, Pascau J. Intraoperative computed tomography imaging for dose calculation in intraoperative electron radiation therapy: Initial clinical observations. PLoS One 2020;15(1):1–12. http://dx.doi.org/10.1371/journal.pone.0227155.

[25] García-Vázquez V, Marinetto E, Guerra P, Valdivieso-Casique MF, Calvo FÁ, Alvarado-Vásquez E, Sole CV, Vosburgh KG, Desco M, Pascau J. Assessment of intraoperative 3D imaging alternatives for IOERT dose estimation. Z Med Phys 2017;27(3):218–31. http://dx.doi.org/10.1016/j.zemedi.2016.07.002.

[26] Ciccotelli A, Carpino S, D'Andrea M, Iaccarino G, Soriani A, Felici G, Benassi M, Strigari L. EP-1573: Validation of a dedicated intra-operative radiotherapy TPS: an innovative tool for image-guided IORT. Radiother Oncol 2016;119:S729–30. http://dx.doi.org/10.1016/S0167-8140(16)32823-7, ESTRO 35, 29 April - 3 May 2016, Turin, Italy.

[27] Alhamada H, Simon S, Philippson C, Vandekerkhove C, Jourani Y, Pauly N, Van Gestel D, Reynaert N. Monte Carlo dose calculations of shielding disks with different material combinations in intraoperative electron radiation therapy (IOERT). Cancer/Radiothérapie 2020;24(2):128–34. http://dx.doi.org/10.1016/j.canrad.2020.02.006.

[28] Schneider F, Bludau F, Clausen S, Fleckenstein J, Obertacke U, Wenz F. Precision IORT – Image guided intraoperative radiation therapy (igIORT) using online treatment planning including tissue heterogeneity correction. Phys Med 2017;37:82–7. http://dx.doi.org/10.1016/j.ejmp.2017.04.017.

[29] Hensley FW. Present state and issues in IORT Physics. Radiother Oncol 2017;12:37. http://dx.doi.org/10.1186/s13014-016-0754-z.

[30] Iaccarino G, Strigari L, D'Andrea M, Bellesi L, Felici G, Ciccotelli A, Benassi M, Soriani A. Monte Carlo simulation of electron beams generated by a 12 MeV dedicated mobile IORT accelerator. Phys Med Biol 2011;56(14):4579. http://dx.doi.org/10.1088/0031-9155/56/14/022.

[31] Valdivieso-Casique MF, Rodríguez R, Rodríguez-Bescós S, Lardíes D, Guerra P, Ledesma MJ, Santos A, nez PI, Vidal M, Udías JM, Otaduy MA, Calama JA, López-Tarjuelo J, Santos-Miranda JA, Desco M, García-Vázquez V, Marinetto E, Pascau J, Calvo F, Illana C. RADIANCE—A planning software for intra-operative radiation therapy. Transl Cancer Res 2015;4(2).

[32] Veronesi U, Orecchia R, Maisonneuve P, Viale G, Rotmensz N, Sangalli C, Luini A, Veronesi P, Galimberti V, Zurrida S, Leonardi MC, Lazzari R, Cattani F, Gentilini O, Intra M, Caldarella P, Ballardini B. Intraoperative radiotherapy versus external radiotherapy for early breast cancer (ELIOT): a randomised controlled equivalence trial. Lancet Oncol 2013;14(13):1269–77. http://dx.doi.org/10.1016/S1470-2045(13)70497-2.

[33] Cavedon C, Mazzarotto R. Treatment planning in intraoperative radiation therapy (IORT): Where should we go? Cancers 2022;14(14). http://dx.doi.org/10.3390/cancers14143532.

[34] Guerra P, Udías JM, Herranz E, Santos-Miranda JA, Herraiz JL, Valdivieso MF, Rodríguez R, Calama JA, Pascau J, Calvo FA, Illana C, Ledesma-Carbayo MJ, Santos A. Feasibility assessment of the interactive use of a Monte Carlo algorithm in treatment planning for intraoperative electron radiation therapy. Phys Med Biol 2014;59(23):7159. http://dx.doi.org/10.1088/0031-9155/59/23/7159.

[35] Favaudon V, Caplier L, Monceau V, Pouzoulet F, Sayarath M, Fouillade C, Poupon M-F, Brito I, Hupé P, Bourhis J, Hall J, Fontaine J-J, Vozenin M-C. Ultrahigh dose-rate FLASH irradiation increases the differential response between normal and tumor tissue in mice. Sci Transl Med 2014;6(245):245ra93. http://dx.doi.org/10.1126/scitranslmed.3008973.

[36] Montay-Gruel P, Acharya MM, Petersson K, Alikhani L, Yakkala C, Allen BD, Ollivier J, Petit B, Jorge PG, Syage AR, Nguyen TA, Baddour AAD, Lu C, Singh P, Moeckli R, Bochud F, Germond J-F, Froidevaux P, Bailat C, Bourhis J, Vozenin M-C, Limoli CL. Long-term neurocognitive benefits of FLASH radiotherapy driven by reduced reactive oxygen species. Proc Natl Acad Sci 2019;116(22):10943–51. http://dx.doi.org/10.1073/pnas.1901777116.

[37] Calvo FA, Serrano J, Cambeiro M, Aristu J, Asencio JM, Rubio I, Delgado JM, Ferrer C, Desco M, Pascau J. Intra-operative electron radiation therapy: An update of the evidence collected in 40 years to search for models for electron-FLASH studies. Cancers 2022;14(15). http://dx.doi.org/10.3390/cancers14153693.

[38] Vozenin M-C, Hendry J, Limoli C. Biological benefits of ultra-high dose rate FLASH radiotherapy: Sleeping beauty awoken. Clin Oncol 2019;31(7):407–15. http://dx.doi.org/10.1016/j.clon.2019.04.001.

[39] Friedl AA, Prise KM, Butterworth KT, Montay-Gruel P, Favaudon V. Radiobiology of the FLASH effect. Med Phys 2022;49(3):1993–2013. http://dx.doi.org/10.1002/mp.15184.

[40] Schuler E, Acharya M, Montay-Gruel P, Loo Jr. BW, Vozenin M-C, Maxim PG. Ultra-high dose rate electron beams and the FLASH effect: From preclinical evidence to a new radiotherapy paradigm. Med Phys 2022;49(3):2082–95. http://dx.doi.org/10.1002/mp.15442.

[41] Esplen N, Mendonca MS, Bazalova-Carter M. Physics and biology of ultrahigh dose-rate (FLASH) radiotherapy: a topical review. Phys Med Biol 2020;65(23):23TR03. http://dx.doi.org/10.1088/1361-6560/abaa28.

[42] Bourhis J, Montay-Gruel P, Gonçalves Jorge P, Bailat C, Petit B, Ollivier J, Jeanneret-Sozzi W, Ozsahin M, Bochud F, Moeckli R, Germond J-F, Vozenin M-C. Clinical translation of FLASH radiotherapy: Why and how? Radiother Oncol 2019;139:11–7. http://dx.doi.org/10.1016/j.radonc.2019.04.008, FLASH radiotherapy International Workshop.

[43] Rahman M, Trigilio A, Franciosini G, Moeckli R, Zhang R, Böhlen TT. FLASH radiotherapy treatment planning and models for electron beams. Radiother Oncol 2022;175:210–21. http://dx.doi.org/10.1016/j.radonc.2022.08.009.

[44] Calvo FA, Ayestaran A, Serrano J, Cambeiro M, Palma J, Meiriño R, Morcillo MA, Lapuente F, Chiva L, Aguilar B, Azcona D, Pedrero D, Pascau J, Delgado JM, Aristu J, Alonso A, Prezado Y. Practice-oriented solutions integrating intraoperative electron irradiation and personalized proton therapy for recurrent or unresectable cancers: Proof of concept and potential for dual FLASH effect. Front Oncol 2022;12. http://dx.doi.org/10.3389/fonc.2022.1037262.

[45] Bourhis J, Sozzi WJ, Jorge PG, Gaide O, Bailat C, Duclos F, Patin D, Ozsahin M, Bochud F, Germond J-F, Moeckli R, Vozenin M-C. Treatment of a first patient with FLASH-radiotherapy. Radiother Oncol 2019;139:18–22. http://dx.doi.org/10.1016/j.radonc.2019.06.019, FLASH radiotherapy International Workshop.

[46] Schiavi A, Senzacqua M, Pioli S, Mairani A, Magro G, Molinelli S, Ciocca M, Battistoni G, Patera V. Fred: a GPU-accelerated fast-Monte Carlo code for rapid treatment plan recalculation in ion beam therapy. Phys Med Biol 2017;62(18):7482. http://dx.doi.org/10.1088/1361-6560/aa8134.

[47] M. DS, et al. A data-driven fragmentation model for carbon therapy GPU-accelerated Monte-Carlo dose recalculation. Front Oncol 2022;12. http://dx.doi.org/10.3389/fonc.2022.780784.

[48] Franciosini G, Battistoni G, Cerqua A, Gregorio AD, Maria PD, Simoni MD, Dong Y, Fischetti M, Marafini M, Mirabelli R, Muscato A, Patera V, Salvati F, Sarti A, Sciubba A, Toppi M, Traini G, Trigilio A, Schiavi A. GPU-accelerated Monte Carlo simulation of electron and photon interactions for radiotherapy applications. Phys Med Biol 2023;68(4):044001. http://dx.doi.org/10.1088/1361-6560/aca1f2.

[49] Luraschi R, Lazzari R, Galimberti V, Rondi E, Bazani A, Corso G, Colombo N, Ricotti R, Fodor C, Winnicki M, Leonardi MC, Jereczek-Fossa BA, Cattani F. Dosimetric study to assess the feasibility of intraoperative radiotherapy with electrons (ELIOT) as partial breast irradiation for patients with cardiac implantable electronic device (CIED). Breast Cancer Res Treat 2018;171:693–9. http://dx.doi.org/10.1007/s10549-018-4878-8.

[50] Bohlen TT, et al. Normal tissue sparing by FLASH as a function of single-fraction dose: A quantitative analysis. Int J Radiat Oncol*Biol*Phys 2022. http://dx.doi.org/10.1016/j.ijrobp.2022.05.038.

[51] Vozenin M-C, De Fornel P, Petersson K, Favaudon V, Jaccard M, Germond J-F, Petit B, Burki M, Ferrand G, Patin D, Bouchaab H, Ozsahin M, Bochud F, Bailat C, Devauchelle P, Bourhis J. The Advantage of FLASH Radiotherapy Confirmed in Mini-pig and Cat-cancer Patients. Clin Cancer Res 2019;25(1):35–42. http://dx.doi.org/10.1158/1078-0432.CCR-17-3375.